# Tuning structure and function in tetra(aniline)-based *rod-coil-rod* architectures

Chinwe U. Udeh,[a] Patrice Rannou,[b] Benjamin P. Brown,[a,c] James O. Thomas,[c,d] and Charl F. J. Faul[a,d*]

[a]School of Chemistry, University of Bristol, Bristol, BS8 1TS (UK)

[b]UMR5819-SPrAM (CEA/CNRS/Univ. J. FOURIER), Institut Nanosciences & Cryogénie (INAC), CEA-Grenoble 17, Rue des Martyrs, 38054 Grenoble Cedex 9 (France)

[c]Bristol Centre for Functional Nanomaterials, Centre for NSQI, University of Bristol, Tyndall Avenue, Bristol, BS8 1FD (UK)

[d]Bristol Centre for Nanoscience and Quantum Information, University of Bristol, Tyndall Avenue, Bristol, BS8 1FD (UK)

charl.faul@bristol.ac.uk

## Table of Contents

# NMR

## TANI-E₃-TANI



**Figure S1** ¹H NMR spectrum of **TANI-E₃-TANI** (LEB state) in DMSO-$d_6$

$^1$H NMR (400 MHz, DMSO-$d_6$, 25°C) δ ppm 9.62 (s, 2 H), 7.76 (s, 2 H), 7.67 (s, 2 H), 7.63 (s, 2 H), 7.38 (d, J=8.98 Hz, 4 H), 7.11 - 7.17 (m, 4 H), 6.85 - 7.00 (m, 24 H), 6.67 (t, J=7.33 Hz, 2 H), 2.24 (t, J=7.33 Hz, 4 H), 1.53 - 1.63 (m, 4 H), 1.28 - 1.35 (m, 4 H).
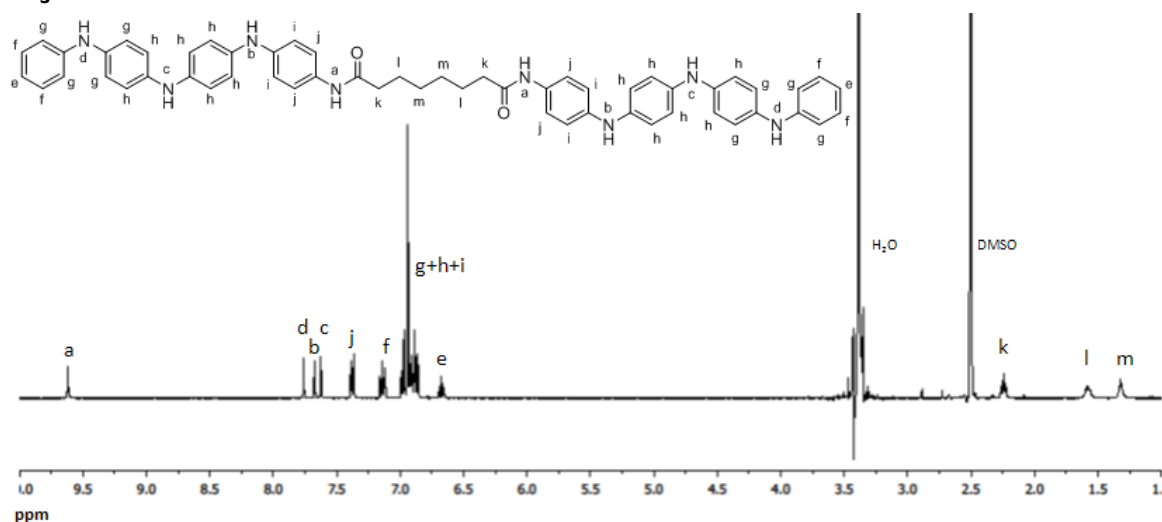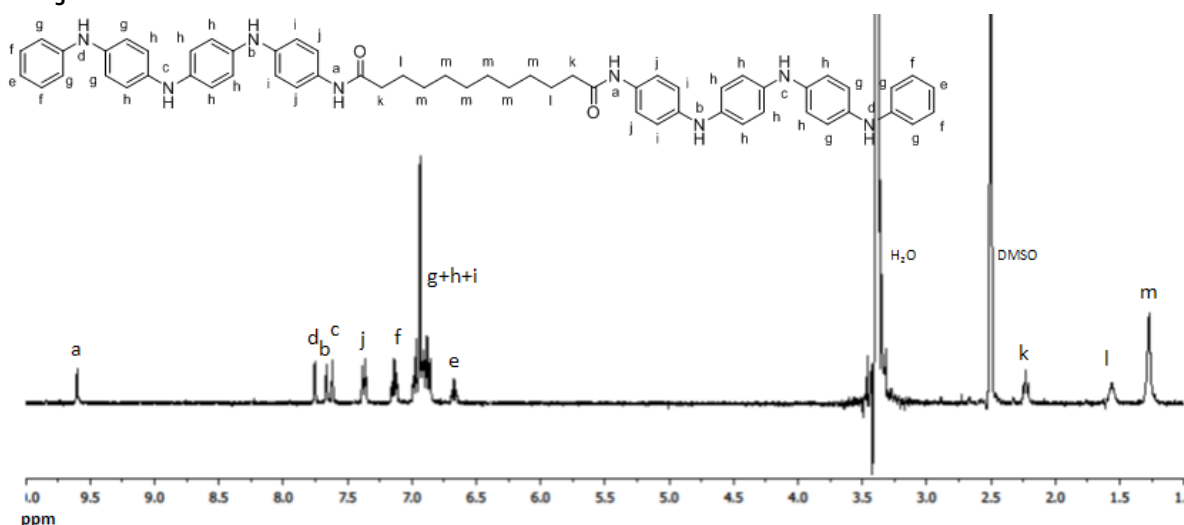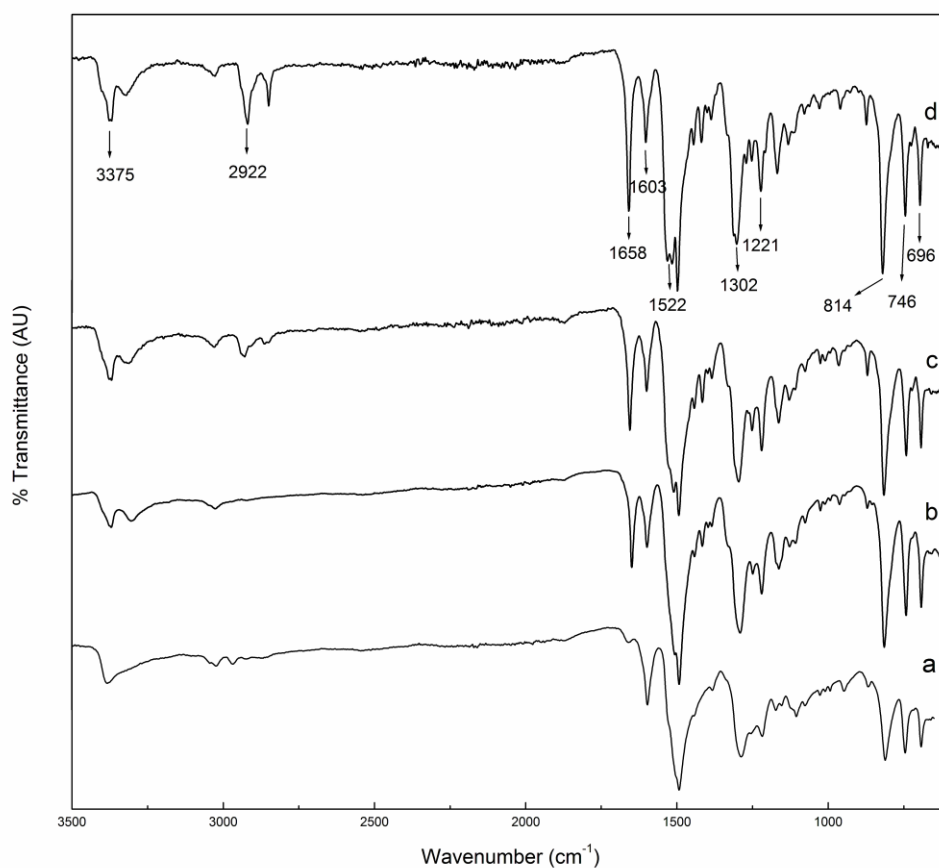
## TANI-E₅-TANI



**Figure S2** ¹H NMR spectrum of **TANI-E₅-TANI** (LEB state) in DMSO-$d_6$

$^1$H NMR (400 MHz, DMSO-$d_6$, 25°C) δ ppm 9.60 (s, 2 H), 7.75 (s, 2 H), 7.66 (s, 2 H), 7.61 (s, 2 H), 7.38 (d, J=8.80 Hz, 4 H), 7.14 (t, J=15.00 Hz, 4 H), 6.85 - 7.02 (m, 24 H), 6.68 (t, J=14.00 Hz, 2 H), 2.24 (t, J=1.00 Hz, 4 H), 1.51 - 1.62 (m, 4 H), 1.28 (br. s., 12 H). The proton signals of the benzene rings appear at 6.67-7.76 ppm. The peaks that appear at 1.28-2.24 ppm are assigned to the methylene protons (*k, l, m*) in the alkyl segment of the *rod-coil-rod* architecture. The peak at 9.6 ppm is assigned to the active proton of the N-H proton of the amide moiety (*a*).[1]

## FT-IR Spectroscopy



**Figure S3** FT-IR spectra of the LEB states of (a) TANI, (b) **TANI-E$_1$-TANI**, (c) **TANI-E$_3$-TANI**, and (d) **TANI-E$_5$-TANI**.

**Table S1** Detailed assignment of the IR vibration frequencies of **TANI-E$_n$-TANI** (EB state)

|  | TANI | TANI-E$_1$TANI | TANI-E$_3$-TANI | TANI-E$_5$-TANI |
|---|---|---|---|---|
| **C=O** | - | 1649 | 1655 | 1656 |
| **N-H (amide)** | - | 3382 | 3380 | 3379 |
| **N-H (amine)** | 3299 | 3309 | 3309 | 3288 |
| **-CH$_2$** | - | 3029 | 3033, 2930, 2850 | 3030, 2918, 2849 |
| **C=C (Quinoid)** | 1595 | 1597 | 1595 | 1596 |
| **C=C (Benzenoid)** | 1495 | 1510 | 1510 | 1512 |
| **C-N** | 1302 | 1297 | 1298 | 1301 |
| **N=Q=N** | 1168 | 1169 | 1167 | 1169 |
| **Q = quinoid** | | | | |

It is noteworthy that with the longer alkyl chain, higher wavenumbers (from 1649 to 1656 cm$^{-1}$) are observed for C=O (amide). Although very small changes, the trend is opposite for the N-H (amide).

3

## UV-Vis Spectroscopy
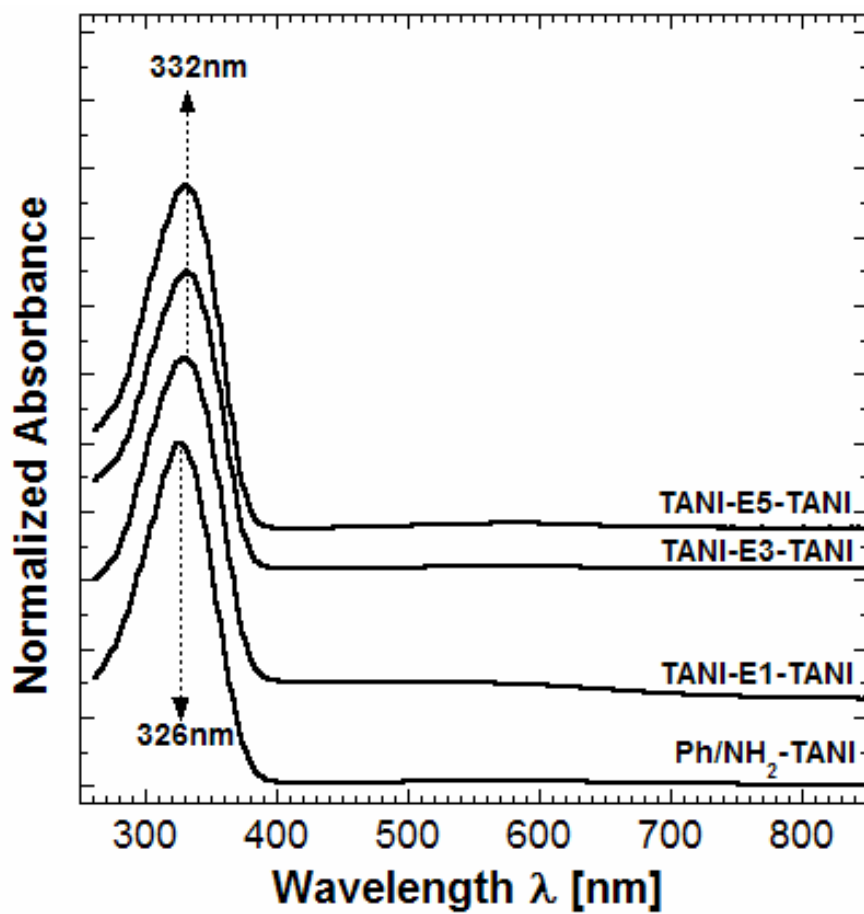


**Figure S4** Solution-state UV-Vis spectra (in DMSO) of Ph/NH$_2$ TANI and **TANI-E$_n$-TANI** in their LEB states.

## Thermal Properties of TANI-based materials

The thermal properties of TANI-based materials were studied by TGA. The TGA curves are shown in **Figure S5**, indicating two degradation stages (under nitrogen atmosphere). TANI and **TANI-E$_1$-TANI** (with the shortest alkyl spacer) have similar thermograms. The first degradation occurred between 200 and 500 °C with 55% weight loss for TANI and **TANI-E$_1$-TANI** and about 77% weight loss for **TANI-E$_3$-TANI** and **TANI-E$_5$-TANI**. This is attributed to the TANI backbone and the alkyl spacer. The second degradation occurred between 500 and 780 °C and is attributed to a further degradation of the TANI segment.
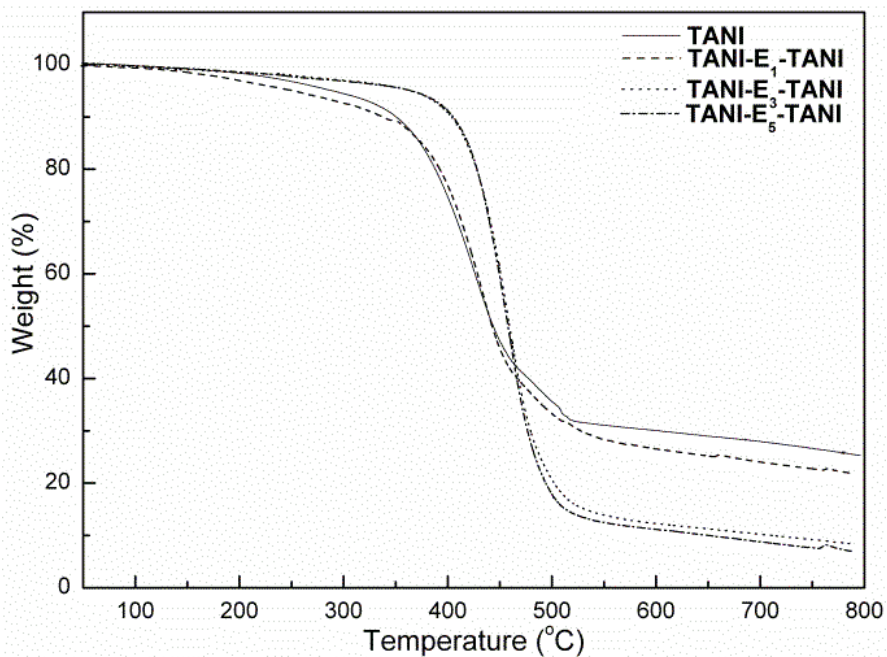


**Figure S5** TGA thermograms (under N$_2$ atmosphere) Ph/NH$_2$ TANI and **TANI-E$_n$-TANI** in their EB states

**Table S2** Weight loss (%) of **TANI-E$_n$-TANI** *rod-coil-rod* architectures at various temperatures

| Weight loss (%) at various temperatures | | | | | | | |
|---|---|---|---|---|---|---|---|
| TANI-based materials | 200°C | 300°C | 400°C | 500°C | 600°C | 700°C | 800°C |
| TANI-E$_1$-TANI | 2.7 | 6.5 | 18.1 | 64.7 | 73 | 75.5 | 77.9 |
| TANI-E$_3$-TANI | 1.4 | 2.5 | 6.9 | 75.3 | 88 | 90 | 91.6 |
| TANI-E$_5$-TANI | 1.5 | 3.1 | 7 | 78 | 89 | 90.9 | 93.1 |

## Microstructures

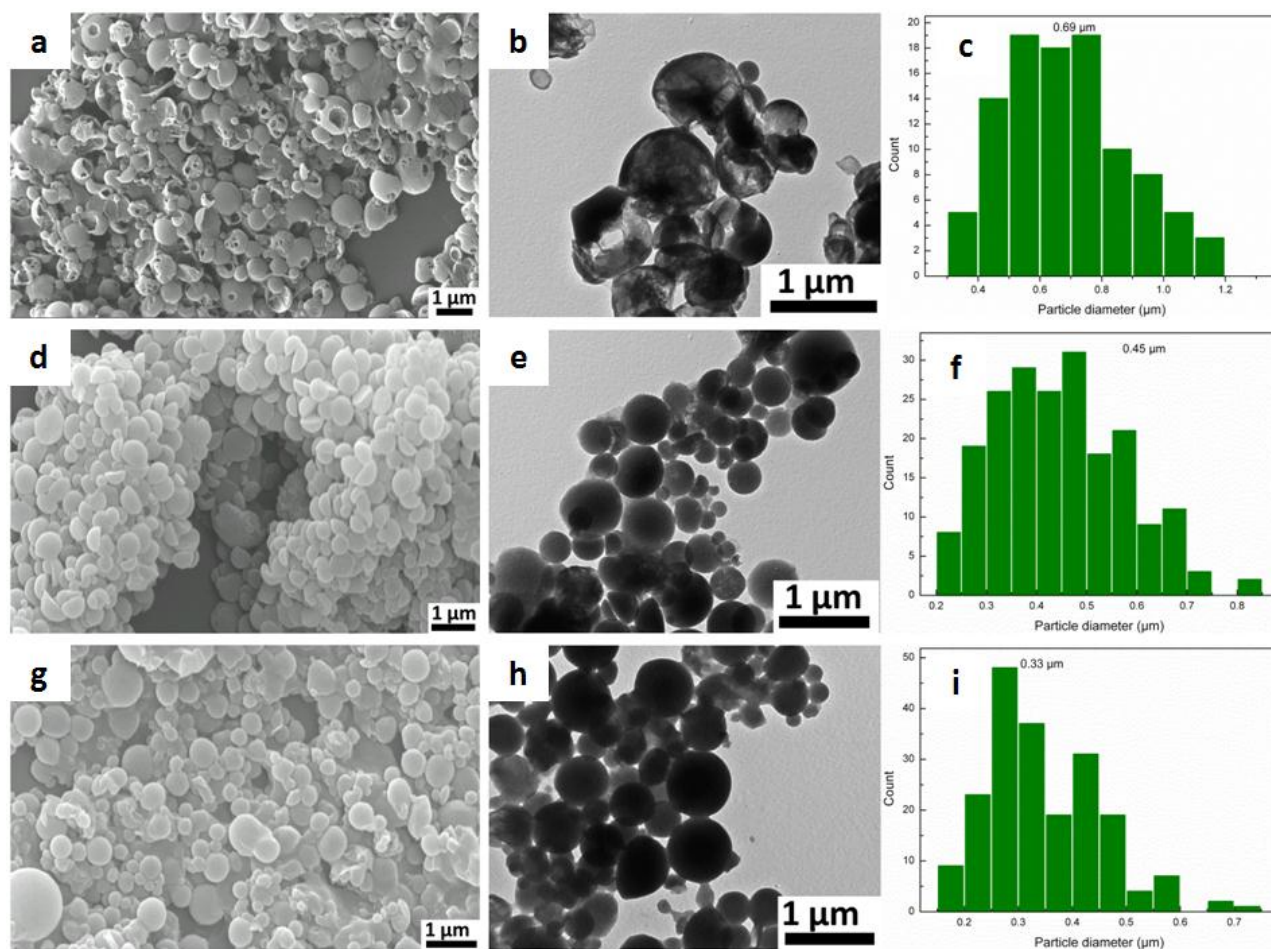## SEM-Microstructures in the (semiconducting) EB state
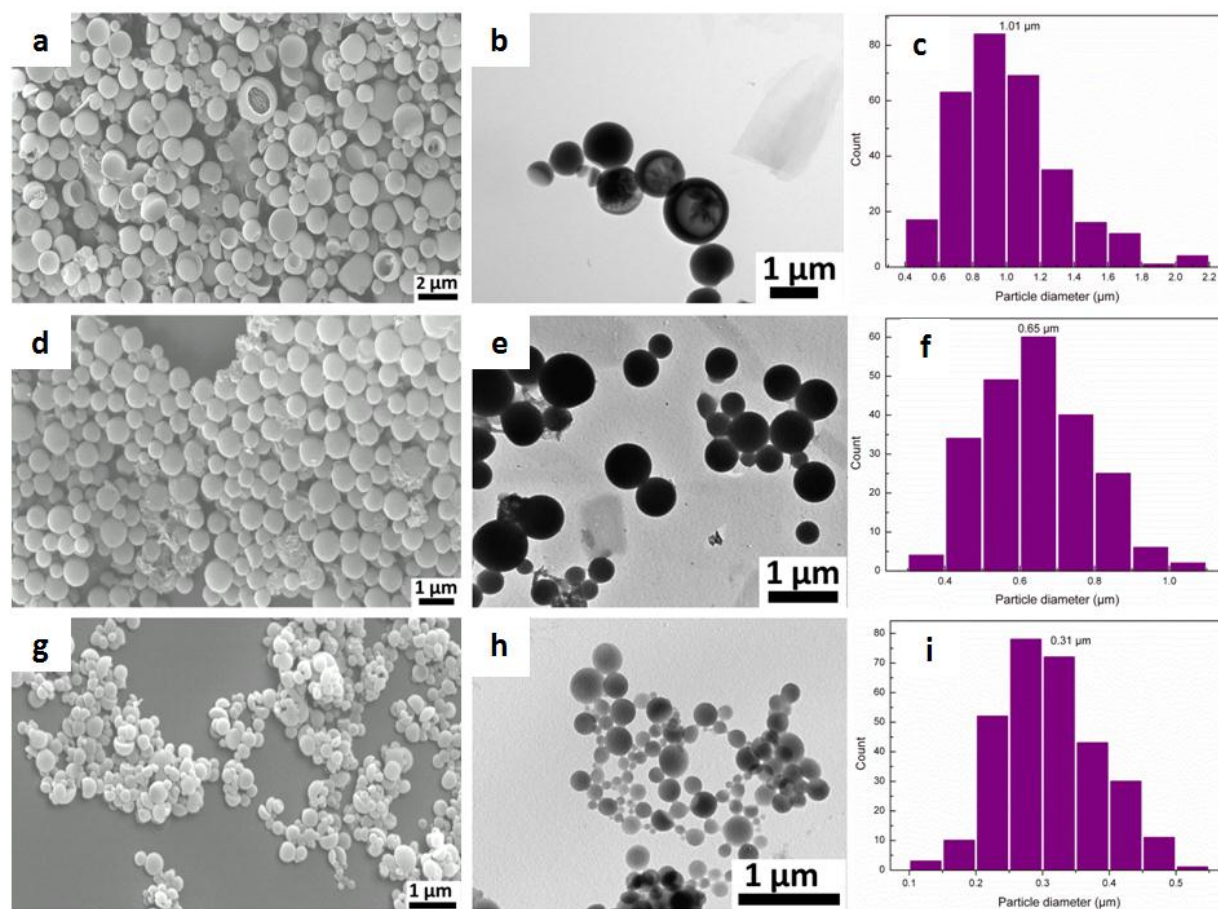


**Figure S6** SEM and TEM images of semiconducting *rod-coil-rod* self-assembled structures cast from a THF/water processing medium. **TANI-E$_1$-TANI** (a and b), **TANI-E$_3$-TANI** (d and e) and **TANI-E$_5$-TANI** (g and h), with corresponding histograms of particle size distributions (c, f and i).

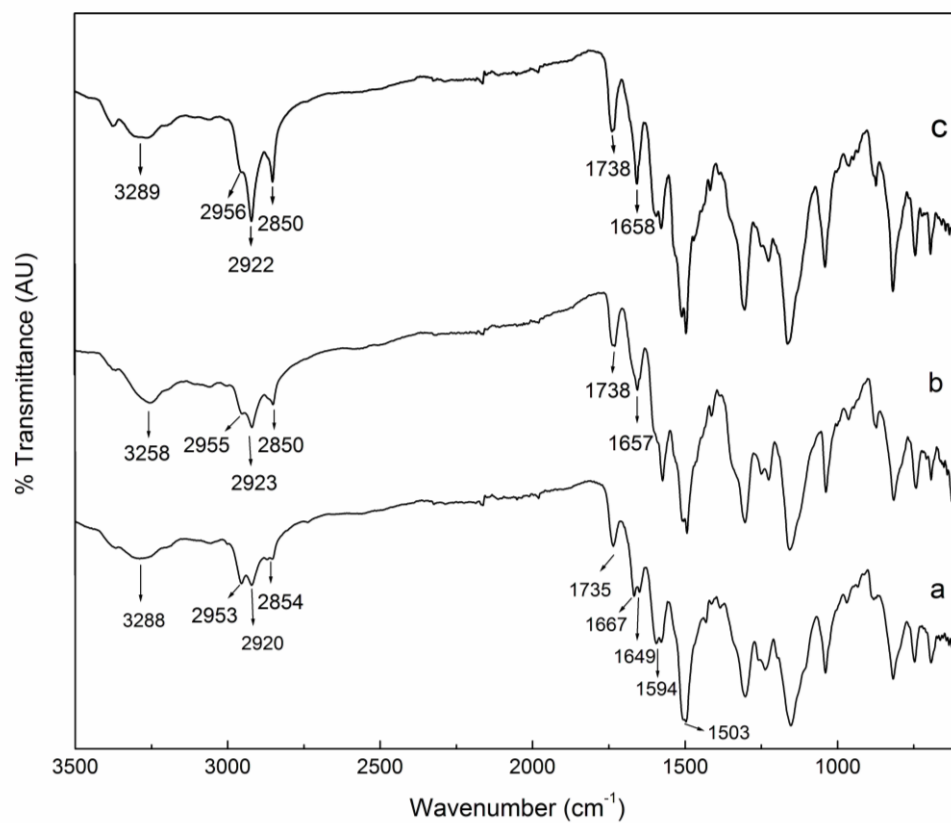## IR-Microstructures in the (semiconducting) EB state
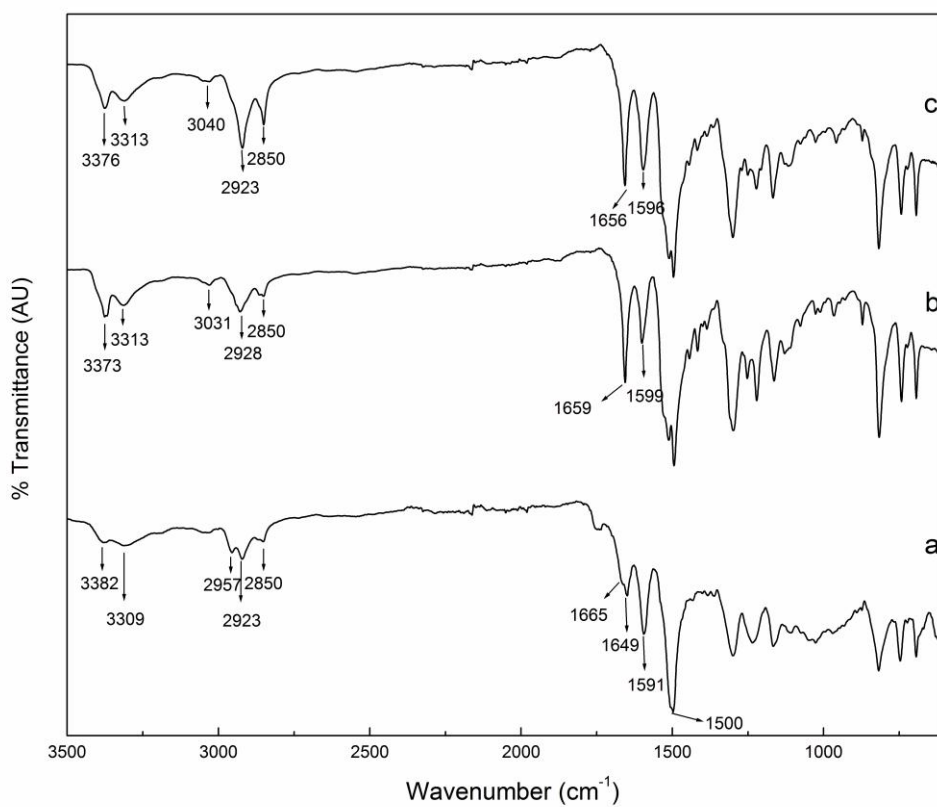


**Figure S7** FT-IR spectra of semiconducting *rod-coil-rod* self-assembled structures from a THF/water processing medium (a) **TANI-E$_1$-TANI**, (b) **TANI-E$_3$-TANI**, and (c) **TANI-E$_5$-TANI**

## SEM-Microstructures in the (conducting) ES state



**Figure S8** SEM and TEM images of CSA-doped conducting *rod-coil-rod* supramolecular conducting microstructures cast from a THF/0.1M aqueous CSA processing medium (a and b) **TANI-E$_1$-TANI**[CSA]$_x$, (d and e) **TANI-E$_3$-TANI**[CSA]$_x$ (g and h) **TANI-E$_5$-TANI**[CSA]$_x$ and corresponding histograms of particle size distributions (c, f and i).

8

## IR-Microstructures in the (conducting) ES state



**Figure S9** FT-IR spectra of CSA-doped *rod-coil-rod* supramolecular conducting materials self-assembled structures cast from a THF/0.1M aqueous CSA processing medium (a) **TANI-E$_1$-TANI**[CSA]$_x$ , (b) **TANI-E$_3$-TANI**[CSA]$_x$ and **TANI-E$_5$-TANI**[CSA]$_x$ (c).

## TEM

Sample preparation:

A sample was pipetted onto a carbon coated TEM grid and blotted with filter paper to remove excess solvent. The TEM grid was placed in a Gatan Model 626DH cryo transfer specimen holder, which was then placed in the Gatan Model 626DH cryo transfer workstation. The tip of the Gatan model 626 DH cryo transfer specimen holder holding the TEM grid was cooled to liquid nitrogen temperature. The cryo transfer specimen holder was then connected to a Gatan Model 900 SmartSet Cold Stage Controller, where the temperature was monitored. When the temperature reached -170 ºC, the cryotransfer specimen holder was taken out of cryotransfer workstation, and quickly transfered to the Jeol 2010 HiRES 200kv Transmission Electron Microscope for imaging.
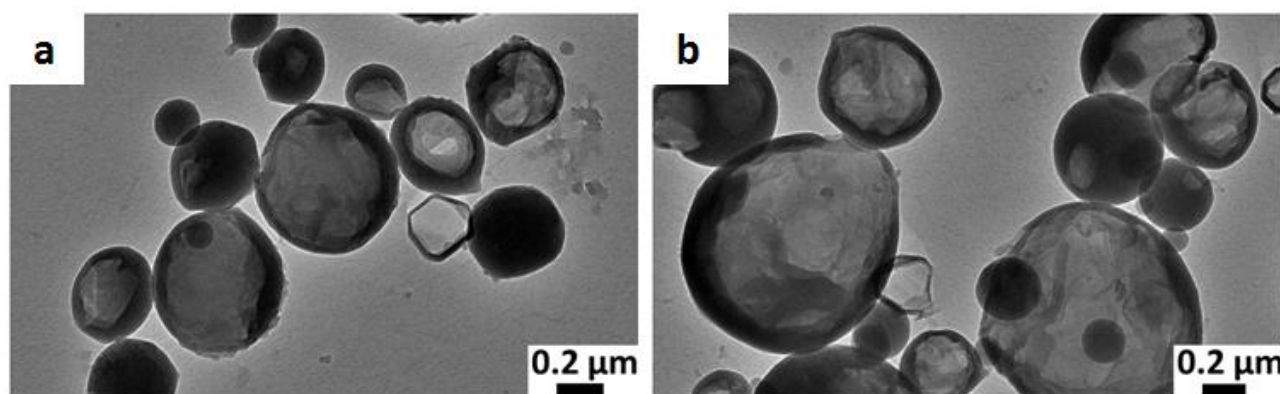


**Figure S10**. TEM images of aggregates of **TANI-E$_1$-TANI**[CSA]$_{0.5}$ prepared by adding 0.1M CSA (1mL) to the oligomer solution in THF.

The morphology of the self-assembled structures obtained from TEM (under cyogenic conditions) were the same as the aggregates formed by drop-casting on a carbon-coated TEM grid, which confirmed that the self-assembly and aggregate formation occurs within the processing medium and not upon drying.

## Conductive AFM

I-V spectra and AFM height and current images were obtained on a MultiMode (Bruker Corp.) AFM using the PeakForce TUNA™ mode. Three I-V spectra were taken on and off each particle; the raw curves are shown in **Figure S12**. Only 2 curves are displayed for **TANI-E$_5$-TANI** as tip-sample drift meant the AFM tip wasn't in contact with the particle for the final spectrum. The averaged curves are displayed in **Figure S13**, and a background curve is inset. All background curves on the gold substrate were identical, with the current signal rapidly reaching saturation at the current sensitivity setting used to probe the particles.
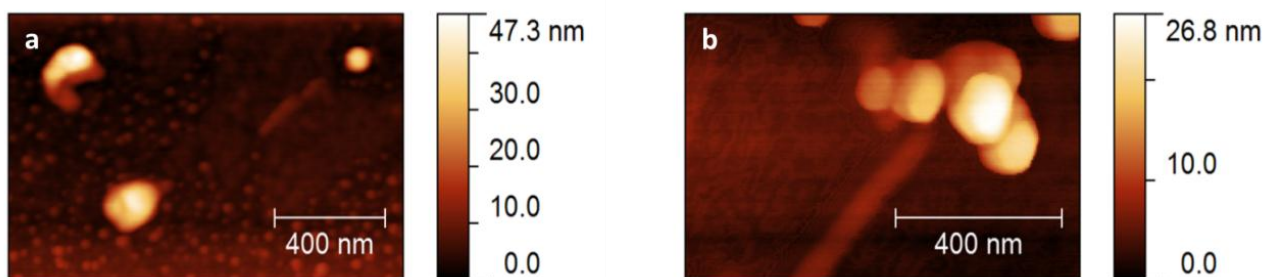


**Figure S11** Typical AFM height images of collapsed vesicular structures, *e.g.* in the top left of (a), and solid spheres (b) from the self-assembly of **TANI-E$_1$-TANI**[CSA]$_{0.5}$.

11
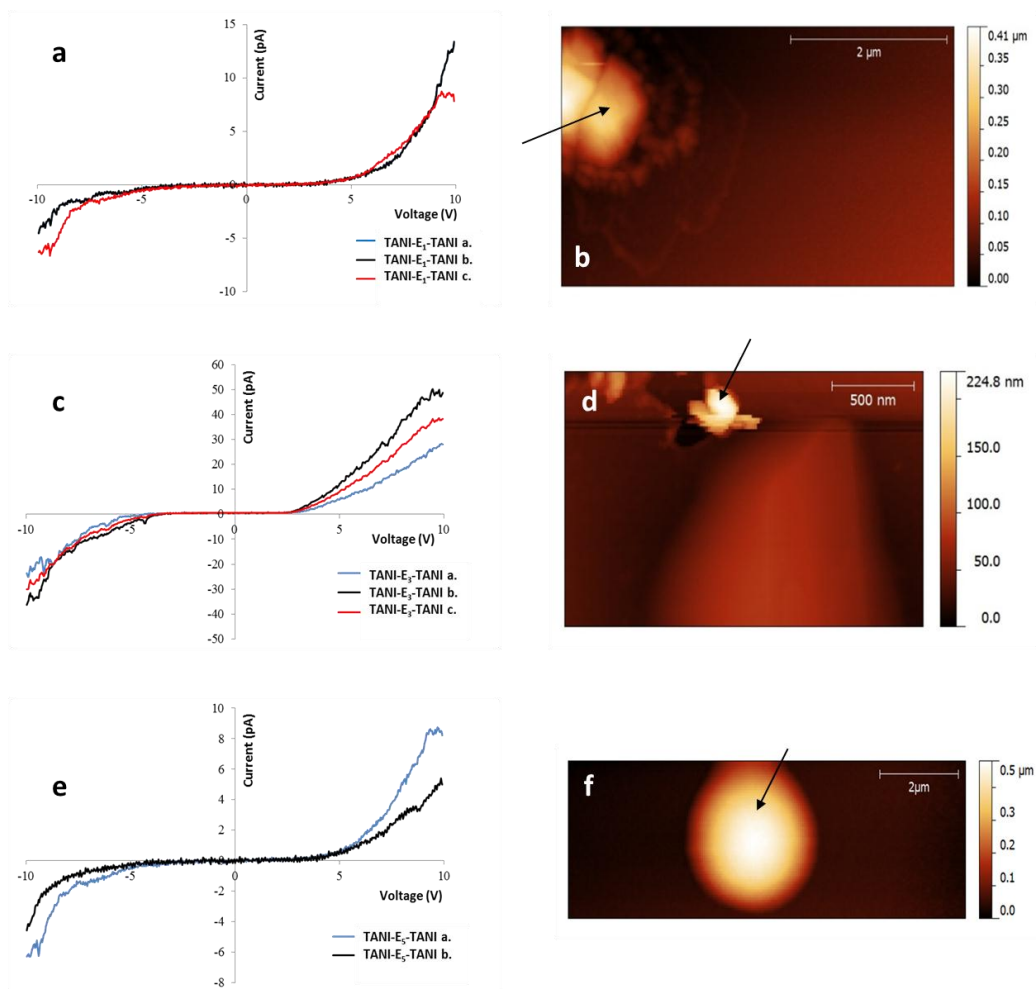
**Figure S12** (a), (c) and (e) show I-V spectra of **TANI-E$_n$-TANI**[CSA]$_{0.5}$ microstructures (b), (d) and (f) are the corresponding AFM height images; arrows indicate the approximate location of the I-V measurements.
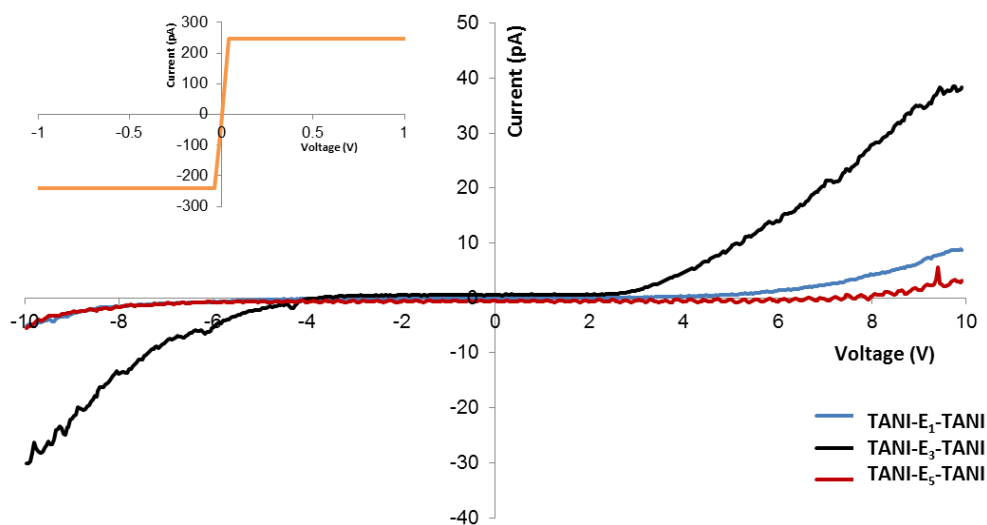


**Figure S13** Averaged I-V spectra for **TANI-E$_1$-TANI**[CSA]$_{0.5}$ (blue), **TANI-E$_3$-TANI**[CSA]$_{0.5}$ (black), and **TANI-E$_5$-TANI**[CSA]$_{0.5}$ (red). Inset: Typical I-V spectrum of gold substrate.

## References

(1)     Yang, Z.; Wang, X.; Yang, Y.; Liao, Y.; Wei, Y.; Xie, X. *Langmuir* **2010**, *26*, 9386.